Available online at www.sciencedirect.com
ScienceDirect
Journal of the European Ceramic Society 30 (2010) 2515–2523
www.elsevier.com/locate/jeurceramsoc

Fully densified zircon co-doped with iron and aluminium prepared by sol–gel processing

W.P.C.M. Alahakoon [a,b], S.E. Burrows [b,*], A.P. Howes [b], B.S.B. Karunaratne [a], M.E. Smith [b], R. Dobedoe [b]

[a] *Department of Physics, University of Peradeniya, Sri Lanka*
[b] *Department of Physics, University of Warwick, Gibbet Hill Road, Coventry CV4 7AL, UK*

Received 25 January 2010; received in revised form 4 May 2010; accepted 16 May 2010
Available online 9 June 2010

Abstract

A sol–gel technique has been used to prepare Fe and Al doped zircon. Structural properties have been studied by X-ray diffraction, nuclear magnetic resonance, scanning electron microscopy and transmission electron microscopy (TEM). Fully densified zircon was produced with high zircon yield and promising microstructures. The presence of Fe promotes zircon formation, while Al improves densification. The zircon phase starts to form at 1215 °C, with almost single phase zircon obtained at 1400 °C when heated for 1 h. Densification increases very significantly (to 99.7% of theoretical density) when the holding time was increased to 48 h from 1 h. TEM micrographs reveal a crystalline grain boundary phase containing some Fe and Al.

PACS: 81.05Je; 81.20Fw

Keywords: A. Sol–gel processing; B. Microstructure; B. Electron microscopy; $ZrSiO_4$

1. Introduction

Zircon ($ZrSiO_4$) has attractive properties which give a role in the manufacture of refractories and as robust enamels and glazes. It has a high resistance to melt corrosion, excellent thermal shock resistance, good chemical stability and mechanical strength at high temperatures as well as low coefficient of thermal expansion, low thermal conductivity and low oxygen diffusivity.

Although natural zircon sand is highly abundant it often contains several impurities leading to poor densification in sintered bodies. Various synthetic gel routes have been reported in the literature[1–9] in order to produce highly pure and fully densified zircon based ceramics. It is believed that a sol–gel route can produce homogeneous starting powders which densify easily producing controlled microstructures; this would increase the range of end uses of zircon to include oxygen barrier coatings. Another advantage of the sol–gel approach is the ability to control dopant levels more accurately. Several research groups have tried to incorporate metal ions such as iron,[1–3,10,11] vanadium[12–18] and praseodymium[19–21] into the structure of zircon during its synthesis. This has primarily been done in order to study the effect of dopants on pigmentation. Relatively little attention has been given to the possibility of using dopants to control the microstructure of synthetic zircon, which is the primary motivation for studying doped zircons in this work.

Conclusions reached in the literature concerning the actual location of dopant cations and their valence in the zircon lattice[15–18,22,23] lack consistency. During the synthesis of iron coral (a zircon based pigment) by coprecipitation routes, Llusar et al.[3] observed that iron mainly appears to be in two different forms: (i) segregated, forming Fe_2O_3 aggregates of different morphology and sizes or (ii) as micron sized Fe_2O_3 particles adsorbed or encrusted on the surface of the bigger zirconia monoliths. Carreto et al.[24] concluded from Mossbauer studies that only a small fraction of iron is incorporated into the zircon structure as paramagnetic Fe^{3+} species while the remaining Fe^{3+} cations form magnetic α-Fe_2O_3 particles which are trapped within the zircon matrix. Berry et al.[25] also have studied

* Corresponding author.
E-mail address: s.e.burrows@warwick.ac.uk (S.E. Burrows).

0955-2219/$ – see front matter © 2010 Elsevier Ltd. All rights reserved.
doi:10.1016/j.jeurceramsoc.2010.05.011

Table 1
Bulk densities, calculated densities and porosities, measured porosities, crystalline phases and the zircon yields of the sintered bodies for different sintering temperatures and times with a heating rate of 600 °C/h.

	Starting powder	900 °C – 1 h	1215 °C – 1 h	1400 °C – 1 h	1400 °C – 5 h	1500 °C – 1 h	1400 °C – 48 h	1500 °C – 48 h
Density[a] (g cm^{-3})	–	–	–	4.45	4.49	4.56	4.63	4.55
Calculated density[b] (g cm^{-3})	–	–	4.63	4.65	4.66	4.66	4.66	4.59
Calculated porosity[b] (%)	–	–	–	4.3	3.6	2.1	0.6	0.8
SEM observed porosity (%)	–	–	–	–	4–5	2–3	0.5	0.5
XRD phases[c]	No crystalline phases	TZ, Sˆ	Z, TZ	Z	Z	Z	Z	Z, MZ
Zircon yield[d] (%)	–	–	94.8	97.0	98.3	98.3	97.7	90.1

[a] The estimated accuracy of the density is ±0.005 g cm^{-3}.
[b] Based on the zircon yield and theoretical densities of 4.68 g cm^{-3} for zircon and 3.76 g cm^{-3} for equimolar zirconia and silica.
[c] Z, zircon; TZ, tetragonal-ZrO_2; MZ, monoclinic-ZrO_2; S, Silica; ˆ, traces.
[d] Zircon yield is as calculated using Eq. (1). This should be regarded as indicative rather than strictly quantitative.

the inclusions of α-Fe_2O_3 together with discrete paramagnetic Fe^{3+} species within the zircon structure. He has shown that iron-doped zircon containing low concentrations of iron (<0.2 mass%) contains Fe^{3+} in low symmetry rhombic sites together with inclusions of α-Fe_2O_3. In materials with higher iron content (>0.2 mass%) the Fe^{3+} occupies higher symmetry sites and the amount of included α-Fe_2O_3 increases. All agree that Fe doping enhances the formation of zircon at a lower temperature than undoped zircon.

It has been documented that 5% Fe dopant is the optimum amount for promotion of zircon formation.[1] In this work highly pure and fully densified zircon bodies have been produced using two dopants, replacing 1% of the initial 5% Fe dopant with Al^{3+}. This follows observations that zircon densifies on firing when in contact with alumina. 4 mol% Fe^{3+} and 1 mol% Al^{3+} doped zircon was synthesized by a sol–gel technique using ferric chloride and aluminium isopropoxide as dopant precursors. Thermal evaluation of the powders was by differential thermal analysis (DTA) and thermogravimetric analysis (TGA), and the sintered bodies were analyzed by means of powder X-ray diffraction (XRD), nuclear magnetic resonance (NMR), scanning electron microscopy (SEM) and transmission electron microscopy (TEM). The densities of the sintered ceramics are more than 99% of the theoretical density and have a high zircon yield of about 98%.

2. Experimental

2.1. Sample preparation

Zirconium propoxide (Aldrich – 70 wt% in 1-propanol) and tetraethoxysilane – TEOS (Aldrich – 98%) were used as the precursors for ZrO_2 and SiO_2, respectively. 0.004 mol of $FeCl_3$ was dissolved in ethanol and added to a mixture of ethanol and 0.1 mol of TEOS. 0.1 mol of zirconium propoxide was added and the mixture refluxed for 120 h at 80 °C. A shorter reflux time gave rise to a less homogeneous microstructure. 0.001 mol of aluminium isopropoxide was added to distilled water and ethanol, heated to 80 °C. Drops of propionic acid were introduced until the aluminium isopropoxide was fully dissolved. Both mixtures were then combined and refluxed for a further hour while stirring, remaining slightly acidic throughout. Once dried, the precursor obtained was ground into a fine powder, calcined, attrition milled and dried. It was then pressed uniaxially (50 MPa) into pellets and sintered in air with a heating rate of 600 °C/h, with varying maximum temperatures and times, shown in Table 1.

2.2. Sample characterization

Densities of the pellets were measured using the Archimedes principle. Differential thermal analysis (DTA) and thermogravimetric analysis (TGA) of the samples were carried out using Stanton Redcroft apparatus in static air up to 1500 °C and 1000 °C, respectively, at a ramp rate of 10 °C/min. Finely powdered quartz was used as a reference.

Powder XRD patterns were recorded on a Bruker AXS D-50 diffractometer with Cu K_α radiation, covering a range of $10° \leq 2\theta \leq 70°$ in steps of 0.02° 2θ. The formation rate of zircon in the powders obtained was calculated by the approximate

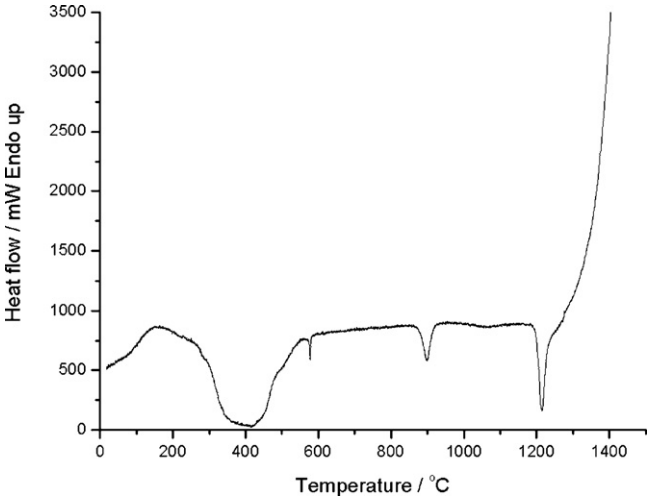

Fig. 1. DTA graph of co-doped precursor powder.

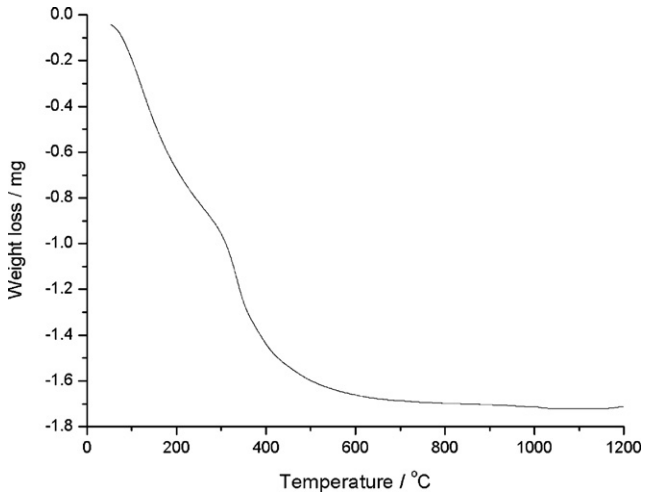

Fig. 2. TGA graph of co-doped precursor powder.

formula[26]:

$$\alpha_{Zr} = \frac{I_{Zr(200)}}{I_{Zr(200)} + I_{m(111)} + I_{m(11-1)} + I_{t(111)}} \quad (1)$$

where I is the peak intensity of XRD and the numbers in parentheses are the plane indices. Subscripts 'Zr', 'm' and 't' stand for $ZrSiO_4$, monoclinic-ZrO_2 and tetragonal-ZrO_2, respectively.

^{29}Si magic angle spinning (MAS) NMR spectra were obtained on Varian-Chemagnetics Infinity Plus spectrometer (7.05 T) operating at 59.62 MHz for ^{29}Si using a Bruker 7.5 mm double bearing MAS probe. The samples were spun at 4 kHz and a 1.5 μs pulse was used to induce a magnetisation tip of $\sim\pi/4$ and a recycle delay of 10 s that produced fully relaxed spectra. Tetramethylsilane (TMS) was used as the chemical shift reference at 0 ppm.

Morphology and elemental analysis of the samples were carried out on a JCM-6100 scanning electronic microscope equipped with energy-dispersive X-ray micro-analyser. Spec-

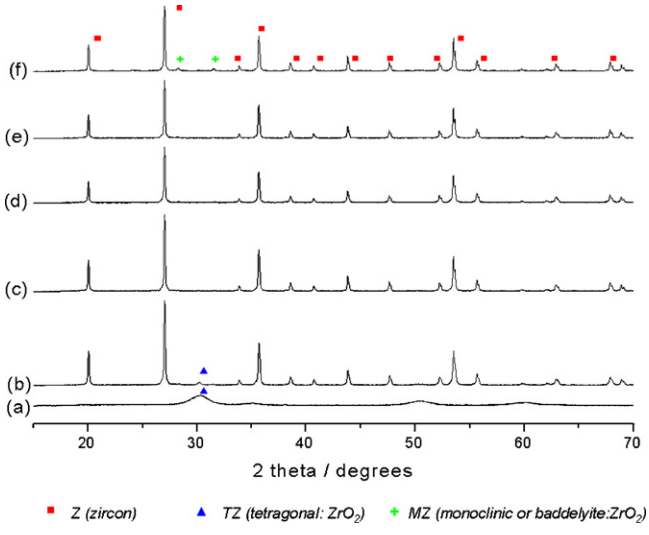

Fig. 3. X-ray diffraction patterns of the Fe and Al doped powders heated at different temperatures: (a) 900 °C for 1 h, (b) 1215 °C for 1 h, (c) 1400 °C for 1 h, (d) 1500 °C for 1 h, (e) 1400 °C for 48 h and (f) 1500 °C for 48 h.

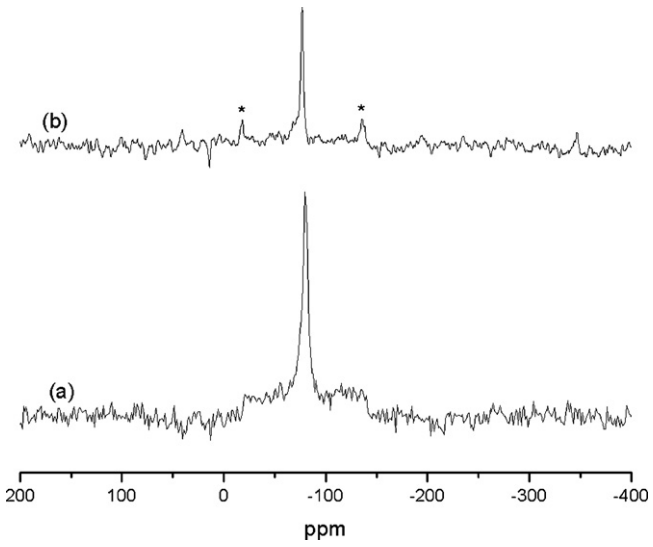

Fig. 4. ^{29}Si MAS NMR spectra for the Fe and Al doped sample sintered at: (a) 1215 °C for 1 h and (b) 1500 °C for 48 h.

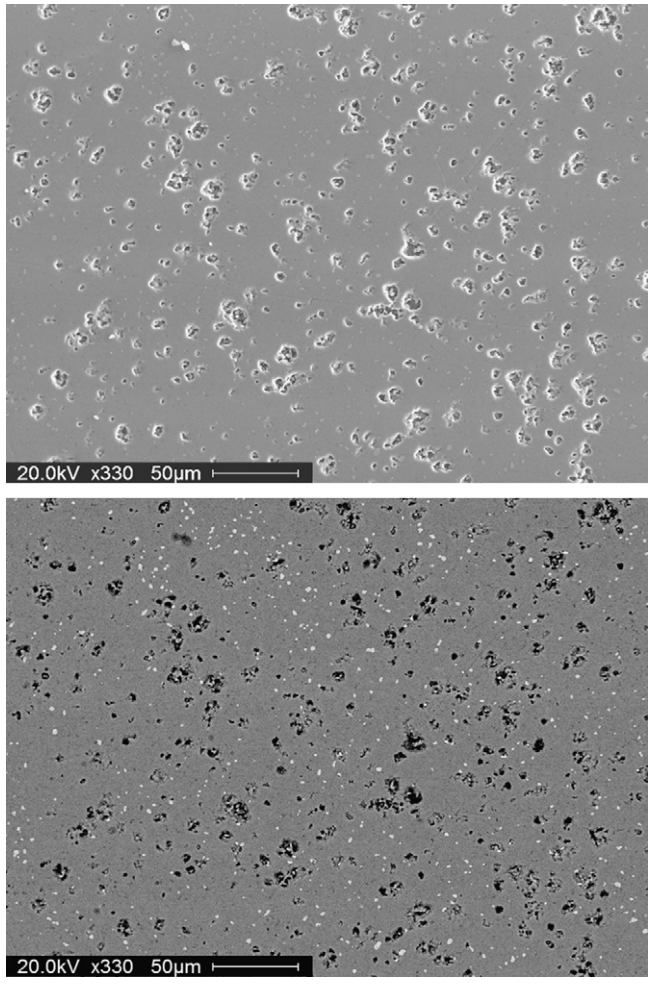

Fig. 5. Secondary (above) and backscattered (below) micrographs of the Fe and Al doped sample sintered at 1400 °C for 5 h.

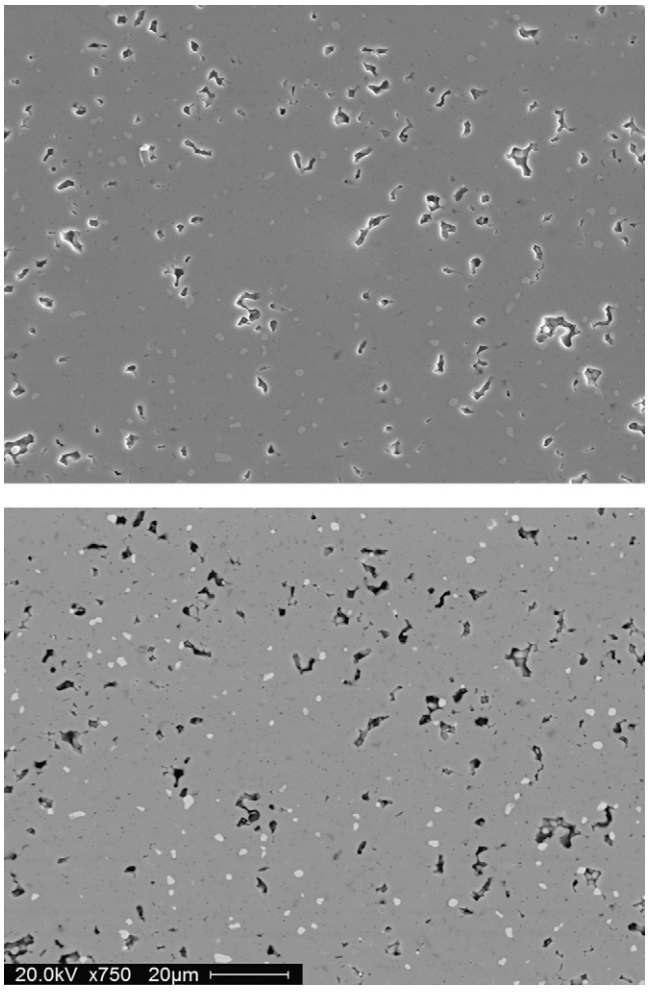

Fig. 6. Secondary (above) and backscattered (below) micrographs of the Fe and Al doped sample sintered at 1500 °C for 1 h.

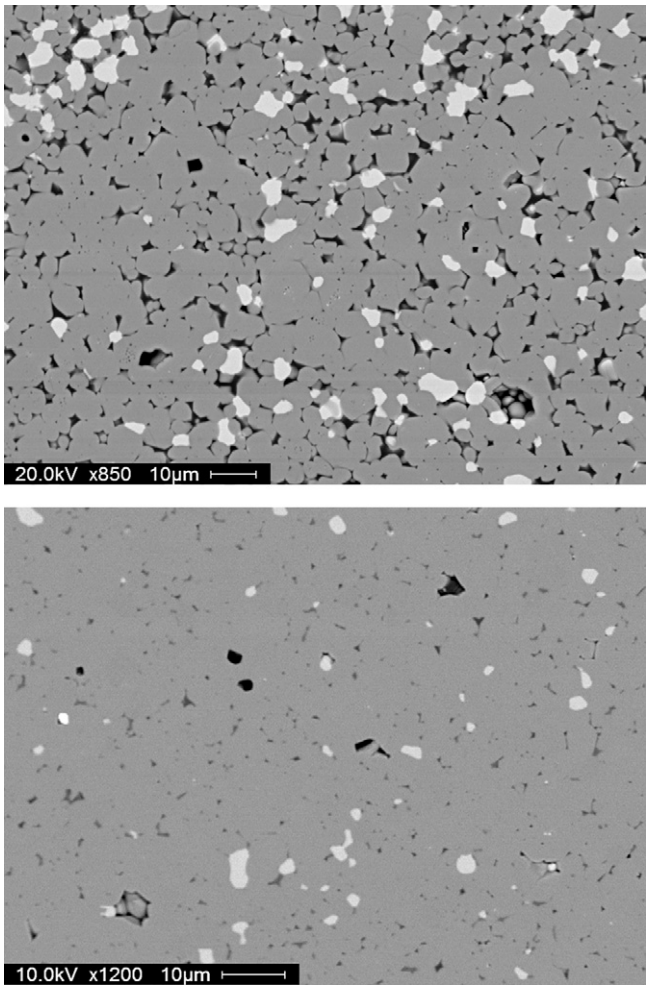

Fig. 7. Backscattered micrographs of the Fe and Al doped sample sintered at 1500 °C for 48 h (above), and at 1400 °C for 48 h (below).

imens were mounted in a Bakelite sample holder and polished with diamond suspension down to 1 μm. Conducting samples were prepared by gold sputtering.

TEM investigations were carried out using a JEOL 2000 RX transmission electron microscope. Samples were cut into small slices and polished on both sides with SiC paper and then with diamond paste down to 1 μm. To obtain the final thinning down to electron transparency the samples were mounted on a 3-mm brass ring with a resin and ion milled with an argon flow incoming at 15° and driven by an accelerating voltage of 5 kV. To avoid electrostatic charging in the microscope, a thin gold film was deposited on the samples.

3. Results and discussion

The DTA curve of the doped precursor powder (Fig. 1) shows a broad exotherm centred at 400 °C associated with the decomposition of remaining organic species. The sharp exothermic peak at ∼575 °C arises from the αβ transition of the quartz reference. The exothermic peak at around 900 °C is due to the crystallisation of tetragonal zirconia, identified by XRD. This indicates the exsolution of ZrO_2 from the SiO_2 network before zircon formation. A final peak at ∼1215 °C is due to the crystallisation of zircon, as identified by XRD. An undoped sample prepared at the same time showed crystallisation of tetragonal zirconia occurring at 900 °C and crystallisation of zircon at ∼1400 °C.

The TGA curve (Fig. 2) is consistent with this interpretation of the DTA data with little mass loss above 600 °C. A 5-h calcining hold at 600 °C was therefore used to remove unwanted volatile species.

Pellets were heated to selected temperatures based on the thermal analysis data, and density values and XRD patterns recorded. The zircon yields (from Eq. (1)), crystalline phases, measured density, porosity and theoretical density and porosity (based on the zircon yield) obtained for different sintering temperatures and times are given in Table 1.

According to these data one can observe that the density has increased with both temperature and holding time. By considering both density values and zircon yield, the best temperature and holding time is 1400 °C for 48 h which gives 99.4% of theoretical density and has a zircon yield of 97.7%; SEM observations confirm that the porosity in this case is about 0.5%. These microstructures have a homogeneous distribution of phases

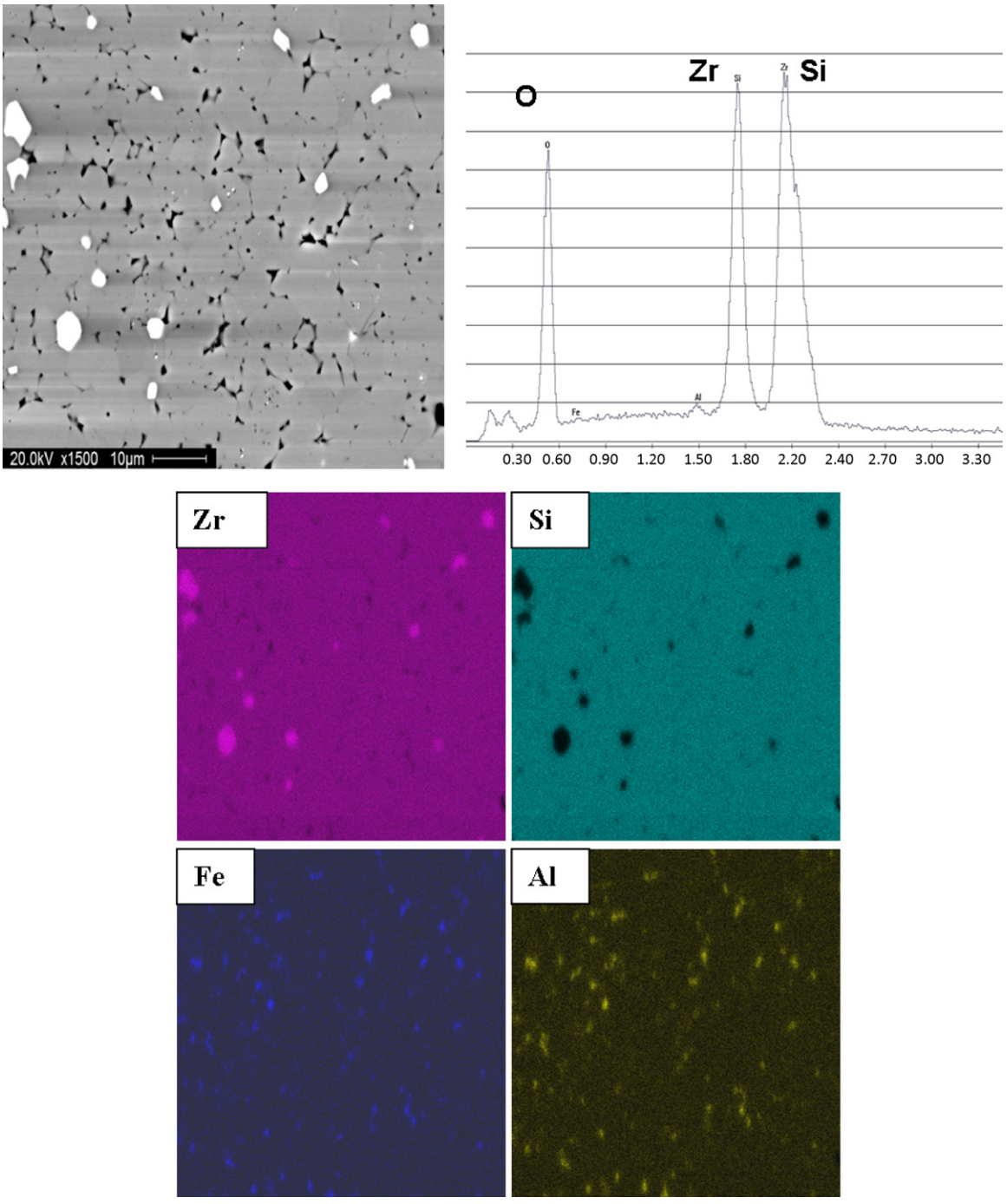

Fig. 8. SEM micrograph, EDX spectrum and the mapping of the same field of the Fe and Al doped sample sintered at 1400 °C for 48 h.

which are consistent throughout. There is a slight reduction in both density and yield when sintered at 1500 °C for 48 h, probably due to the presence of monoclinic zirconia formed through dissociation. These results indicate that the presence of Fe^{3+} has promoted crystallisation of the zircon phase, in agreement with literature results,[2,6,11] whereas the presence of Al^{3+} has enhanced the sintering process, combining to produce a high density ceramic.

XRD analysis of the samples sintered for various temperatures and times are shown in Fig. 3. From 900 °C onwards the XRD patterns clearly reveal the presence of tetragonal zirconia, these peaks disappearing with onset of zircon formation at 1215 °C. Evidence to support the theory that zircon is formed from amorphous silica and monoclinic zirconia, and that zircon will only form when the tetragonal to monoclinic conversion has started, is still unclear. Single phase zircon could be obtained at 1400 °C when heated just for 1 h. Continued heating at 1500 °C for 48 h was accompanied by a small diffraction peak due to monoclinic zirconia (Fig. 3(f)). This indicates that zircon is slightly dissociated at this time and temperature. The behaviour of sol–gel prepared zirconia is in contrast to that of naturally occurring bulk zirconia which is stable at room temperature

in the monoclinic form, converting to tetragonal at 1170 °C on heating and undergoing inversion back to monoclinic on cooling at 1040 °C. It is known that several effects can influence the equilibrium between the tetragonal and monoclinic forms and the conversion between the two phases. For example, reducing the particle size is thought to increase the relative stability of the tetragonal phase.[27] ^{17}O MAS NMR studies[28,29] of the sol–gel preparation of zirconia have shown that mixtures of these two polymorphs form with the relative amounts varying with preparation conditions and heat treatment. In sol–gel formed ZrO_2–SiO_2 xerogels, the nature of the zirconia formed can be readily characterized by ^{17}O MAS NMR[30–32] with in some cases metastable tetragonal zirconia being observed. This is consistent with the observations here which could be due to a number of factors such as the stabilizing effect of SiO_2 or the zirconia forming interstitially between zircon particles and being constrained in size.

Fig. 4 shows the ^{29}Si MAS NMR spectra obtained for the co-doped samples heated for 1215 °C for 1 h and 1500 °C for 48 h. The samples were acid washed before the experiment in order to avoid signal loss due to broadening through interaction with paramagnetic iron present within the sample. The ^{29}Si NMR spectrum of the sample sintered at 1215 °C for 1 h shows a sharp peak at around −81.4 ppm. As suggested by XRD data, this peak is due to the presence of zircon with only Si–O–Zr type bonds such that all the SiO_4 units are Q^0 species.[33] This is as expected for zircon as there are no Si–O–Si bridging bonds between the tetrahedra. With further heating, i.e. 1500 °C for 48 h, there is no change in the site for the Si atom, but a decrease in peak sharpness indicating either a reduction in crystallinity or some small unaveraged interaction with paramagnetic iron species. There is some other circumstantial evidence that this paramagnetic interaction has changed since the spinning sidebands formed are different (marked as * in Fig. 4(b)), and in the 1500 °C sample there also appears to be some broader underlying intensity. In this sample the peak has shifted as well to about −78.4 ppm, which could be due to a transferred hyperfine interaction, as has been observed in some ^{29}Si MAS NMR peaks of V^{4+} doped zircon.[18] The intensity of this peak is stronger than that observed for the 1215 °C sample probably due to the increased formation of zircon (according to XRD it is about 90%).

SEM micrographs of the polished samples are displayed in Figs. 5–10. At higher magnification, they reveal a three phase microstructure consisting of zircon (grey contrast), zirconia (bright contrast) and silica (dark contrast). Porosity is in the form of intergranular pores, the degree of porosity decreasing with increasing time and temperature of the heat treatment. The samples sintered at 1400 °C for 5 h and 1500 °C for 1 h have observed porosity of about 4–5% (Fig. 5) and 2–3% (Fig. 6), respectively. These observed porosity values, measured from SEM images, support the findings of the densification studies. Both these samples have a lower percentage of zirconia (∼1.5%) compared to the samples sintered for longer times, confirming the high zircon yield calculated from the XRD data. Correspondingly there is reduced intergranular phase, leading to less contrast between zircon grains. An increased grain boundary phase could compromise the high temperature properties in the samples sintered for longer times, if it is glassy.

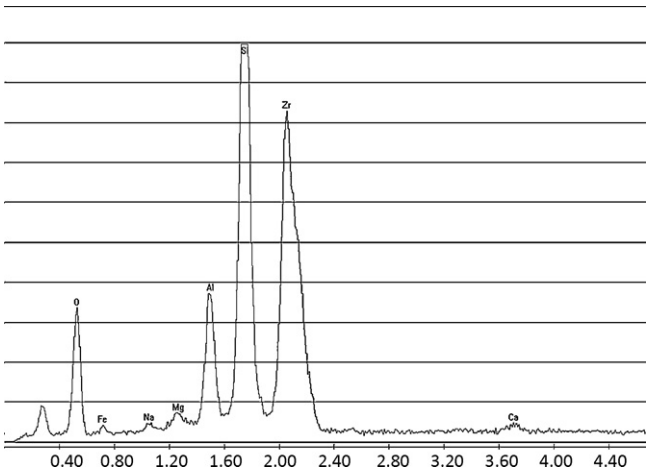

Fig. 9. EDX spectrum of the glassy phase.

Samples sintered at 1400 °C for 48 h have an excellent microstructure. Extending the holding time from 1 h to 48 h at 1400 °C increases the apparent density and decreases open porosity, imparting an almost fully dense microstructure (with a porosity of about 0.5%). Intergranular zirconia (mostly monoclinic according to XRD) is apparent in the backscattered image, distributed randomly with irregular forms and sizes. Fig. 7 shows the contrast in images between this and the sample sintered at 1500 °C for 48 h which has a more porous microstructure, again showing monoclinic zirconia precipitates (about 6%) indicating dissociation. This confirms work done by Rendtorff et al.,[34] where decomposition of zircon occurs at a relatively low temperature in the presence of alumina. Pure zircon is thought to dissociate at 1673 °C, the dissociation temperature lowering with impurities, and to a lesser extent with increase in grain size.[35] It is important to note that all micrographs show samples free from microcracking, due to the absence of tetragonal zirconia which will undergo a phase change to monoclinic on cooling with a significant associated change in volume, typically 9%.

The improved sinterability of the doped zircon is thought to be due to the presence of Al^{3+}, which reduces the viscosity of the intergranular glassy phase, enabling silicon cations to diffuse more quickly through the zirconia grains to form zircon. The effect of this liquid phase sintering is to eliminate internal pores more effectively, increasing the bulk density of the final ceramic. In the literature it has been reported that during heating of zircon–mullite composites, zircon will be in equilibrium with a glassy phase[36]; alumina present in the mixture will be dissolved in this glassy phase and will precipitate out as mullite during cooling, although no mullite was detected by XRD in these samples due to the small amounts of Al present. This would suggest that there is a possibility of producing a densified ceramic with a crystalline grain boundary phase which does not degrade at high temperatures. The absence of a glassy grain boundary phase should improve high temperature creep properties, as shown in Si–Al–O–N diphasic and monophasic ceramics.[37]

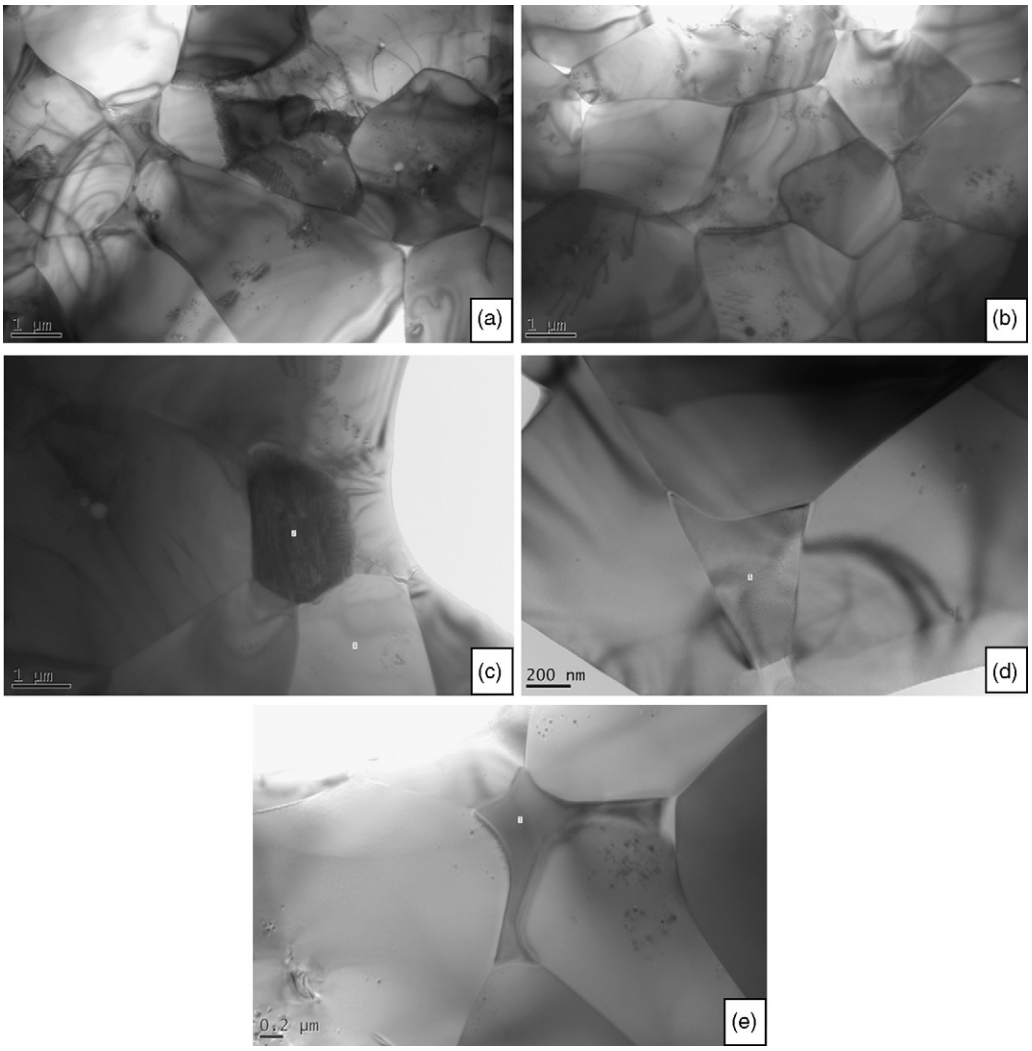

Fig. 10. TEM micrographs of the Fe and Al doped sample sintered at 1400 °C for 48 h.

In order to understand the distribution of the phases, EDX mapping was performed for the sample sintered at 1400 °C for 48 h and is displayed in Fig. 8, along with the spectrum of the same field. One can clearly see the distribution of the main dopants Fe and Al where they are present in the crystalline grain boundaries. The presence at the triple points of some glassy phase composed of Al, Si, Zr and O, with Na, Mg, Fe and Ca present in trace amounts is confirmed by the EDX analysis in Fig. 9.

TEM micrographs of the sample sintered for 1400 °C for 48 h are shown in Fig. 10(a)–(e). Homogeneous zircon grains could be observed throughout the sample. Some of the zircon grains are imaged containing dislocation networks and small angle grain boundaries. Moreover there are some strain contours present. Fig. 10(c) shows some twinning inside the zirconia grains in a very fine scale. An EDX spectrum reveals that the dark region is a zirconia grain inside the zircon matrix (Fig. 11). A significant feature observed in these samples is the crystalline grain boundary phase (region 1 shown in Fig. 10(d) and (e)), confirmed by electron diffraction. An EDX spectrum reveals that this consists of mainly Fe and Al (Fig. 12). From considerations of the molar ratios of Al, Fe and O taken from Fig. 12, and from the sintering temperature of 1400 °C, it is expected that the most likely composition of this grain boundary phase is $Fe_2O_3{\cdot}Al_2O_3$.

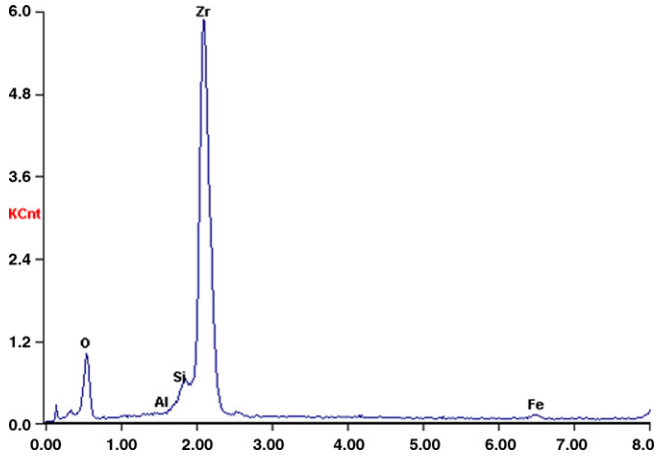

Fig. 11. EDX spectrum of the dark grain in Fig. 10(c).

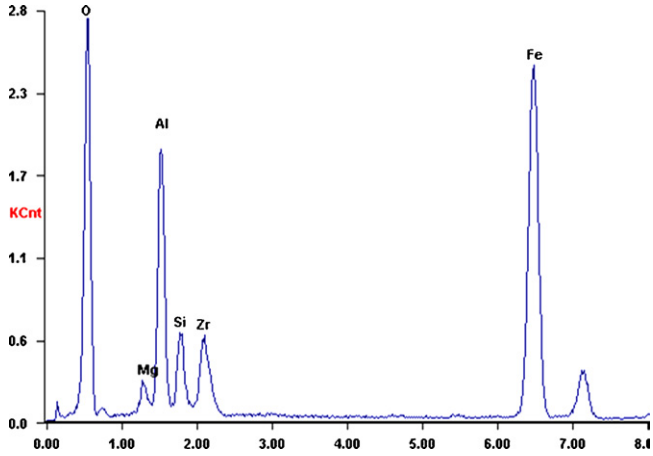

Fig. 12. EDX spectrum of the grain 1 in Fig. 10(d) and (e).

4. Conclusion

A fully densified zircon ceramic, free from microcracking, has been prepared by a sol–gel technique, using Fe^{3+} and Al^{3+} as dopants. The presence of Fe^{3+} promoted the formation of zircon and the presence of Al^{3+} ions has reduced the porosity, leading to a fully dense microstructure after 48 h at 1400 °C. When formed by the sol–gel process, co-doped zirconia powder crystallises first to tetragonal zirconia at 900 °C, converting slowly to monoclinic form with the onset of zircon formation at 1215 °C. Dissociation of the zircon above 1500 °C to give monoclinic zirconia is shown to be dependent on both time and temperature. The formation of a crystalline grain boundary rather than a glassy phase should be beneficial with regards to high temperature creep resistance, whilst the lack of any remaining tetragonal zirconia in the structure precludes any crack formation on cooling, either from thermal mismatch between zircon and zirconia or from the tetragonal to monoclinic zirconia transition with its associated volume change.

Acknowledgements

We would like to acknowledge the support given by the Asian Development Bank to this project. EPSRC, the University of Warwick and AWM/ERDF via the Science City Advanced Materials theme are thanked for their partial support of the NMR facility.

References

1. Cappelletti G, Ardizzone S, Fermo P, Gilardoni S. The influence of iron content on the promotion of the zircon structure and the optical properties of pink coral pigments. *J Eur Ceram Soc* 2005;**25**:911–7.
2. Tartaj P, Gonzalez-Carreno T, Serena CJ, Ocana M. Iron zircon pigments prepared by pyrolysis of aerosols. *J Solid State Chem* 1997;**128**:102–8.
3. Llusar M, Calbo J, Badenes JA, Tena MA, Monros G. Synthesis of iron zircon coral by coprecipitation routes. *J Mater Sci* 2001;**36**:153–63.
4. Llusar M, Calbo J, Badenes JA, Tena MA, Monros G. Environmental and color optimization of mineraliser addition in synthesis of iron zircon ceramic pigment. *Br Cerm Trans* 2000;**99**:14–22.
5. Eppler RA. Kinetics and formation of an iron–zircon pink color. *J Am Ceram Soc* 1979;**62**:47–9.
6. Veytizou C, Quinson JF, Douy AA. Sol–gel synthesis via an aqueous semi-alkoxide route and characterization of zircon powders. *J Mater Chem* 2000;**10**:365–70.
7. Mori T, Yamamura H, Kobayashi H, Mitumura T. Preparation of high purity $ZrSiO_4$ powder using sol–gel processing and mechanical properties of the sintered body. *J Am Ceram Soc* 1992;**75**:2420–6.
8. Shi Y, Huang XX, Yan DS. Effect of natural zircon powder as seeds on the gel synthesis of zircon powder. *Mater Lett* 1994;**21**:79–83.
9. Shi Y, Huang XX, Yan DS. Synthesis and characterization of ultrafine zircon powder. *Ceram Int* 1998;**24**:393–400.
10. Gracia A, Llusar M, Badenes J, Tena MA, Monros G. Encapsulation of hematite in zircon by microemulsion and sol–gel methods. *J Sol–Gel Sci Technol* 2003;**27**:267–75.
11. Ardizzone S, Binaghi L, Cappelletti G, Fermo P, Gilardoni S. Iron doped zirconium silicate prepared by a sol–gel procedure. The effect of the reaction conditions on the structure, morphology and optical properties of the powders. *Phys Chem Chem Phys* 2002;**4**:5683–9.
12. Ardizzone S, Cappelletti G, Fermo P, Oliva C, Scavini M, Scime F. Structural and spectroscopic investigations of blue, vanadium-doped $ZrSiO_4$ pigments prepared by a sol–gel route. *J Phys Chem B* 2005;**109**:22112–9.
13. Valentin C, Munoz MC, Alarcon J. Synthesis and characterisation of vanadium containing $ZrSiO_4$ solid solution from gels. *J Sol–Gel Sci Technol* 1999;**15**:221–30.
14. Torres FJ, Tena MA, Alarcon J. Rietveld refinement study of vanadium distribution in V^{4+}–$ZrSiO_4$ solid solution obtained from gels. *J Eur Ceram Soc* 2002;**22**:1991–4.
15. Demirary T, Nath DK, Hummel FA. Zircon–vanadium blue pigments. *J Am Ceram Soc* 1970;**53**:1–4.
16. Di Gregorio S, Greenblatt M, Pifer JH, Sturge MD. An ESR and optical study of V^{4+} in zircon type crystals. *J Chem Phys* 1982;**76**:2931–7.
17. Xiayou H, Gui-Ku B, Ming-Guang Z. The study of the optical and EPR spectra of V^{4+} in zircon type crystals. *J Phys Chem Solids* 1985;**46**:719–20.
18. Dajda N, Dixon JM, Smith ME, Carthey N, Bishop PT. Atomic site preferences and structural evolution in vanadium-doped $ZrSiO_4$ from multinuclear solid-state NMR. *Phys Rev B* 2003;**67**:0242011–9.
19. Ocana M, Caballero A, Gonzalez-Elipe AR, Tartaj P, Serena CJ. Valence and localization of praseodymium in Pr-doped zircon. *J Solid State Chem* 1998;**139**:412–5.
20. Badenes JA, Vicent JB, Llusar M, Tena MA, Monros G. The nature of Pr–$ZrSiO_4$ yellow ceramic pigment G. *J Mater Sci* 2002;**37**:1413–20.
21. Nero GD, Cappelletti G, Ardizzone S, Fermo P, Gilardoni S. Yellow Pr–zircon pigments. The role of praseodymium and of the mineralizer. *J Eur Ceram Soc* 2004;**24**:3603–11.
22. Cortes EC, Fuente JAM, Moreno JM. Solid solution formation in the synthesis of Fe–zircon. *J Am Ceram Soc* 2004;**4**:612–6.
23. Berry FJ, Eadon D, Holloway J, Smart LE. Iron doped zirconium silicate. Part 1. The location of iron. *J Mater Chem* 1996;**6**:221–5.
24. Carreto E, Pina C, Arriola H, Barahona C, Nava AN, Castano V. Mossbauer study of the structure of Fe–zircon system. *J Radional Nucl Chem* 2001;**50**:453–8.
25. Berry FJ, Eadon D, Holloway J, Smart LE. Iron-doped zircon: the mechanism of formation. *J Mater Sci* 1999;**34**:3631–8.
26. Du C, Yuan Q, Yang Z. Lowering the synthesis temperature of zircon powder by yttria addition. *J Mater Sci Lett* 1999;**18**:965–6.
27. Garvie RC. Stabilization of tetragonal structure in zirconia microcrystals. *J Phys Chem* 1978;**82**:218–24.
28. Bastow TJ, Smith ME, Whitfield HJ. Characterisation of zirconia gels by ^{17}O nuclear magnetic resonance. *J Mater Chem* 1992;**2**:989–90.
29. Chadwick AV, Mountjoy G, Nield VM, Poplett IJF, Smith ME, Strange JH, Tucker MG. Solid-state NMR and X-ray studies of the structural evolution of nanocrystalline zirconia. *Chem Mater* 2001;**13**:1219–29.
30. Dirken PJ, Dupree R, Smith ME. Structural role of zirconium in SiO_2–ZrO_2 gels – evidence from ^{17}O NMR. *J Mater Chem* 1995;**5**:1261–3.
31. Pickup DM, Mountjoy G, Wallidge GW, Newport RJ, Smith ME. Structure of $(ZrO_2)_x(SiO_2)_{1-x}$ xerogels ($x = 0.1$, 0.2, 0.3 and 0.4) from FTIR, ^{29}Si and ^{17}O MAS NMR and EXAFS. *Phys Chem Chem Phys* 1999;**1**:2527–33.
32. Armelao L, Gross S, Muller K, Pace G, Tondello E, Tsetsgee O, Zattin A. Structural evolution upon thermal heating of nanostructured

inorganic–organic hybrid materials to binary oxides MO_2–SiO_2 (M = Hf, Zr) as evaluated by solid-state NMR and FTIR spectroscopy. *Chem Mater* 2006;**103**:6019–30.

33. MacKenzie KJD, Smith ME. *Multinuclear solid state NMR of inorganic materials*. Oxford: Pergamon Press; 2002.
34. Rendtorff NM, Garrido LB, Aglietti EF. Thermal shock behavior of dense mullite–zirconia composites obtained by two processing routes. *Ceram Int* 2008;**34**:2017–24.
35. Kaiser A, Lobert M, Teller R. Thermal stability of zircon. *J Eur Ceram Soc* 2008;**28**:2199–211.
36. Hamidouche M, Bouaouadja N, Torrecillas R, Fantozzi G. Thermomechanical behavior of a zircon–mullite composite. *Ceram Int* 2007;**33**: 655–62.
37. Karunaratne BSB, Lewis MH. High temperature fracture and diffusional deformation mechanisms in Si–Al–O–N ceramics. *J Mater Sci* 1980;**15**:449–62.